Check for updates

ORIGINAL ARTICLE

Moisture and frequency dependent conductivity as an obstacle to determining electrical percolation thresholds of cementitious nanocomposites made with carbon nanotubes

Francesco Piana · Marco Liebscher ⦿ · Thomas Köberle · Imen Mechergui

Abstract Impedance spectroscopy was applied to Portland cement and its carbon nanotubes (CNT) composites to measure and describe the electrical conductance phenomena and their dependency on the moisture. Two series of composites were prepared, one with multi-walled, and the other with single-walled CNTs. The percolation concentration was reached only with the single-walled CNTs between 0.10 and 0.25 wt%; it was therefore possible to compare a percolative and a non-percolative system. The kinetic of the drying process was measured in the range of 24 h and described by a decay model with a stretched exponential to be correlated with the composite composition. The polarization phenomena occurring in the materials before and after the moisture removal were modelled with logistic sigmoid and explained by the morphology. In particular, the three found sigmoid were correlated to the polarization phenomena occurring at well-defined structural levels of the specimens. Their mathematical definition was shown to be fundamental for a correct interpretation of the Cole-plots of the real conductivity. Such phenomena presented a peak of intensity at a well define frequency but their effects spread across a broad range of Hertz. Moreover, over the AC frequency of 10 Hz, the conductive effect of the moisture overlapped the conductivity increase caused by the percolative network of the CNT. A dry sample is therefore necessary for accurately evaluating the source of the conductivity, a distinction which is crucially important for sensing applications.

F. Piana (✉) · I. Mechergui
Institute of Macromolecular Chemistry, Academy of Sciences of the Czech Republic v.v.i., Heyrovsky Sq. 2, Prague 6, Czech Republic
e-mail: piana@imc.cas.cz

M. Liebscher (✉) · T. Köberle
Institute of Construction Materials, Technische Universität Dresden, Georg-Schumann-Str. 7, 01062 Dresden, Germany
e-mail: marco.liebscher@tu-dresden.de

1 Introduction

For many years, the introduction of electrically conductive carbon nanofillers, such as carbon nanotubes (CNT) or graphene and their derivates have been of high scientific interest for developing multifunctional nanocomposites with a wide range of mechanical, thermal and electrical properties [1, 2]. The characteristic CNT high aspect ratio is

particularly attractive [3], since it may increase flexural strength, young's modulus, toughness, and fracture energy [4] with very low filler concentration. With slightly higher nanofiller concentration the electrical percolation threshold is reached [5] enabling the creation of multifunctional cement/CNT nanocomposites which can be used for sensing applied mechanical loads [6], inducing electrical heating properties [7], or thermal energy harvesting properties [8]. Finally, cement/CNT sensors were also found to be capable of measuring dynamically varying strains in concrete structures [9]. However, for such applications it must be considered that the CNTs influence not only the resistivity of the material itself but also the conductive mechanism of the composite which is additionally influenced by moisture. In fact, the CNTs increase the electrical conductivity of cementitious composites but also reduce the ionic conductivity [10].

Dielectric cement/CNT composites belong to the field of the heterogeneous material, whose properties were well introduced by Asami and colleagues [11]. In cement/CNT composites the matrix permittivity (ε') is not negligible, unlike most polymer composites, and thus requires more sophisticated interpretative models [12]. Various parameters influence the composite properties beside the concentration, such as the form factors of the filler and the size of the particles [13]. Moreover, the temperature has a complex effect on ε', which decreases from room temperature to 100 °C and then increases rapidly while the dielectric loss due to temperature (ε'') had an even more complicated trend [14]. The influence of the applied stress on the dielectric properties is also fundamental for sensing application. It was observed that the sensibility of properties like impedance on the mechanical stress has a maximum at an optimized filler concentration and is proportional to its degree of dispersion [15]. These studies apply electrochemical impedance spectroscopy to the piezoelectric properties of cement composites to observe the correlations between water content and piezoresistive performances [16]. Specifically, the impedance spectroscopy allows to separate the contributions of the ionic and electric conductivity and their dependency on the hydration time, which also influences the porosity of the cement matrix [17]. Moreover, Díaz and colleagues used impedance spectrometry to show the correlation between the pore diameter and distribution, and filler geometry. [18] An advanced analysis and modelling of the

conductivity in cementitious composites containing conductive fillers therefore enables a fast and deep exploration of the morphology of the bulk. [19] Since the morphology is strictly connected to the thermal conductivity but easy to monitor, conductivity becomes a useful tool to track the preparation of the material [20]. This is particularly crucial in novel curing processes like the Ohmic heating which is noticeably influenced by the filler presence [7, 21].

Often, theoretical models are applied to describe both nanostructures and macro properties of cementitious composites. Bending behaviour of composites with carbon fillers was recently interpreted with the Mori–Tanaka model, to predict the distribution and geometry of the carbon filler and macro properties like hardness and modulus [22], while the strain sensing response of the composites was simulated with a finite element model [23]. For the elaboration of the electrical conductivity in composites, simple parallel and series or the more elaborated cube model, usually reserved to ceramic fillers, were used [24]. The isothermal dependence of the conductivity on the frequency was interpreted by Funke K. and colleagues using the MIsmatch Generated Relaxation for the Accommodation and Transport of IONs (MIGRATION) concept, to define the slope in the log–log plot. [25] This method proved to be inefficient in describing the composite transition from direct to alternate regime observed in this work. A more appropriate model was the interpolation with a simple logistic sigmoid, applied to the logarithm of the conductivity as a function of the logarithm of the frequency. The total curve was the result of the composition of 2 or 3 sigmoid (named α, β, and γ in order of crescent frequency) attributed to the different polarization effects appearing at various levels of the specimen structure [26].

$$\log(\sigma') = \log(\text{DC}) + \sum_{i=\alpha, \beta, \gamma} \frac{\Delta(\log \sigma)_i}{1 - e^{-R_{g,i}\left(\log(f) - \log(P_{f,i})\right)}} \tag{1}$$

where σ' is the real part of the conductivity, f is the frequency in Hertz, DC is the direct current, $\Delta(\log(\sigma_i))$ is the height of the sigmoid, R_g is the growth rate of the function, and P_f is the flexural point that defines the position of the sigmoid on the x-axis. For $f \to 0$, σ' is equal to the DC while for $f \to \infty$, σ' becomes:

$$\log(\sigma') = \log(DC) + \sum_{i=\alpha,\beta,\gamma} \Delta(\log(\sigma_i)) = \log(AC)$$

$$(2)$$

where AC is the alternate current. The choice of logistic sigmoid model was motivated by the observation of the evolution of σ' plot passing from the ideal to the real case. An ideal resistor in an ideal circuit would provide a constant σ', independent on the frequency, in which the AC would be always equal to the DC. An ideal resistor in a real circuit would provide a σ' plot in three sections. A central section in which σ' is directly proportional to the frequency, surrounded by two sections of constant conductivity, caused by the junction at the electrodes. The value at low frequency would be assumed to be the DC value, as mentioned in the previous paragraph, while the value at high frequency would be assumed to be the AC. Finally, the σ' of a real resistor in a real circuit would show a smoother transition, which is more similar to a sigmoid than to a broken line graph (Fig. 1). Moreover, the electrodes are not the only interphases present in a real resistor, especially a composite, which suggested the sum of multiple sigmoid. This approach allowed us to disaggregate, quantify and provide a physical description for the contributions to the σ' graph.
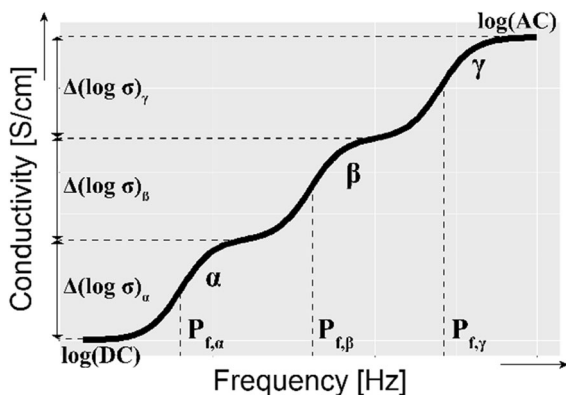

Fig. 1 Schematic representation of the proposed sigmoid model derived from Eq. (1) showing the three sigmoid. The parameter $R_{g,i}$, which is the mathematical derivative of conductivity in the point $P_{f,i}$, was omitted for the sake of clarity

2 Experimental

2.1 Materials and sample preparation

Nanocomposites with 0.01 wt%, 0.10 wt%, 0.25 wt% and 0.50 wt% were prepared. A CEM I 42.5R from Schwenk, Germany was used as binder matrix. Single-walled carbon nanotubes (SWCNT) TUBALL™ from OCSiAl EUROPE, Luxembourg were used. Multi-walled carbon nanotubes (MWCNT) "SMW210" were obtained from SWeNT company (Norman, OK, USA). For all nanocomposites a water to cement ratio of 0.4 was chosen. Samples preparation is based on previous studies by the author [7, 8]. Before preparing the nanocomposites, the CNTs were mixed in deionized water (DI water) via ultrasonication in an iced bath for 5 min at 70% amplitude using a Bandelin Sonopuls 3100 instrument with a VS70T Sonotrode from Bandelin, Germany. To assist the dispersion of the CNT in the DI water, sodium dodecylbenzenesulfonate (SDBS) was used as a surfactant. For all specimen a CNT:SDBS ratio of 1:1 was chosen. After pre-dispersing the CNTs via ultrasonication, the obtained slurries were shear mixed with the cement at room temperature by using a laboratory shear mixer IKA 200 P4 with a R 1381 propeller stirrer for 5 min at 300 rpm. For the dielectric characterization, cylinders (10 mm height × 20 mm diameter) were casted in oiled moulds and preserved in plastic bags to prevent cracking induced by shrinkage. Two days after the preparation, the samples were demoulded and kept in sealed plastic bags until testing.

2.2 Characterization

The dielectric properties of the samples were analysed at an age of 28 days using an impedance spectrometer Alpha- Analyser from Novocontrol Technologies, Montabaur, Germany. Dielectric spectra were measured in a frequency interval of 10^{-1}–10^{7} Hz in air at room temperature ($\sim$ 20 °C). Time dependence was analysed at 60 °C, under N_2 in the range of 24 h every 30 min, in the same frequency range. Data analysis and extrapolation of the function parameters was made with R-language in RStudio software. The method used for the sigmoid deconvolution was iterative, starting from the pristine cement, and then proceeding in order of increasing filler concentration. Consequently, the process was repeated excluding the

incoherent or physically meaningless solutions and monitoring the Residual Sum of Squares (RRS) to determine quality of the fitting. The results were considered acceptable only with RRS < 0.1. Values under 0.01 were reached for most of the samples (Table S.I. 1).

Morphological analysis was carried out by conducting optical microscopy (OM) and scanning electron microscopy (SEM). OM was used to assess the macro dispersion states of the different fillers. Therefore, small pieces of selected samples were impregnated in Epoxy resin and a thin section of 30 μm thickness was prepared. Light transmission analyses were carried out by using a Keyence digital microscope VHX-6000. SEM was performed on fractured surfaces of the nanocomposites by using ESEM, Quanta 250 FEG, FEI, The Netherlands in high pressure mode (4–10 kV: spot 2, 5).

3 Results and discussion

3.1 Morphological analysis

Optical microscopy (OM) was used to assess the macro dispersion states of carbon fillers in the cementitious matrix (Fig. 2). The images clearly reveal common morphological features as well as significant differences in the investigated materials (Fig. 2a, b). Both types of nanocomposites with 0.50 wt% showed a considerable amount of non-dispersed CNT agglomerates which were homogenously distributed throughout the matrix. A content of 0.50 wt% CNT could be considered relatively high, in particular for studies on mechanical properties, but still adequate for electrical applications where a high conductance was desired [27]. The dispersion states of both fillers might be improved with longer ultrasonication times, but the reduction of the agglomerate dimension would be compensated by the ruptures of CNTs reducing their aspect ratio and broadening the statistical distribution of their size [28].

Considering the shape of the CNT agglomerates clear differences could be seen between MWCNT and SWCNT. The MWCNT agglomerates showed a typical spherical shape [29, 30] with diameters of up to 600 μm. For the SWCNT nanocomposites more agglomerates with rather irregular shapes and larger sizes were found [31]. This worse macro scaled CNT dispersion was traced back to a less effective SWCNT dispersion during the applied ultrasonication process in aqueous suspension with SDBS compared to the MWCNTs and indicated a poorer interaction of the SWCNT with the SDBS.

A study of the fractured surfaces via SEM revealed more differences between SWNCT and MWCNT in terms of agglomeration and embedding in the cementitious matrix (Fig. 3). For the MWCNT a densely felted agglomerate well embedded in the cementitious matrix was observed (Fig. 3a). Connected pores were also visible at the surface, especially close to the CNT clusters. It is well accepted that their volume increases with filler content [32, 33]. Both the number of pores and size distribution may increase by the addition of
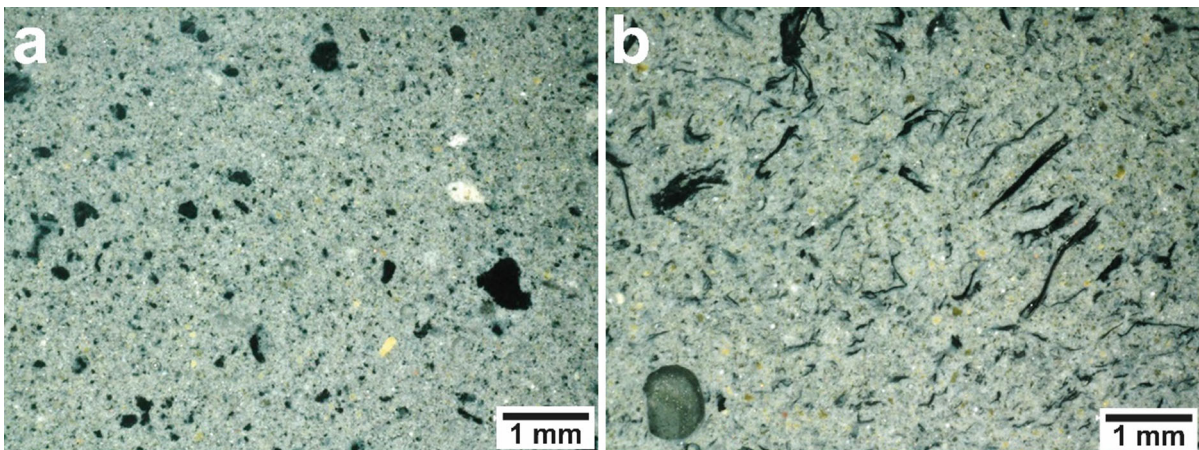

Fig. 2 Optical micrographs of cementitious nanocomposites with 0.50 wt% MWCNT (**a**) and 0.50 wt% SWCNT (**b**). The agglomerated nanomaterial shows as black
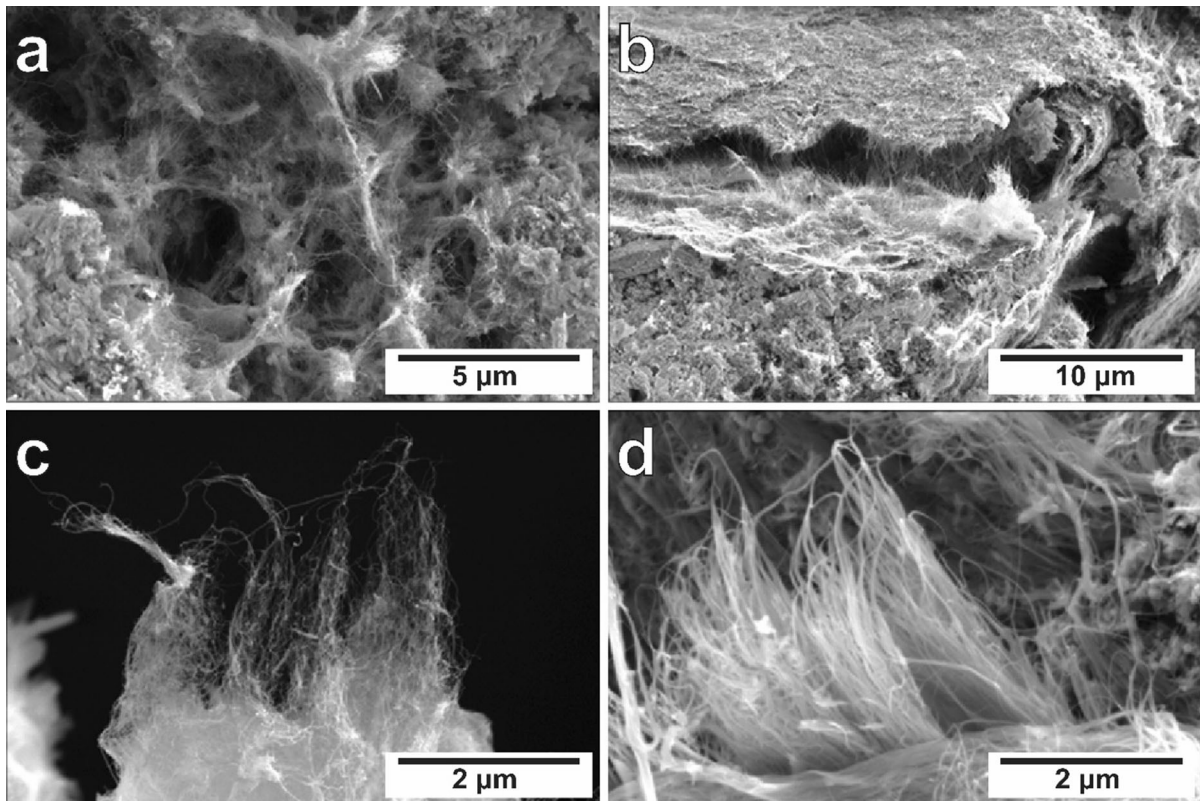
Fig. 3 Scanning electron micrographs of cementitious nanocomposites with 0.50 wt% MWCNT (left) and 0.50 wt% SWCNT (right), at different levels of magnification: overall morphology (top) and detail of the filler (bottom)

nanofillers [34]. Moreover, curing conditions effect pore dimensions [35].

At higher magnification, highly entangled CNTs were also found (Fig. 3c). In particular, for the nanocomposites containing SWCNT, the irregular shaped agglomerates appeared relatively porous and spread longitudinally (Fig. 3b). Within these agglomerates of densely aligned CNTs even clusters longer than 5 μm were found (Fig. 3d). In general, the alignments were observed in short range but no preferential orientation directions were observed in the overall samples; this allows us to assume that the measured specimens were prevalently anisotropic.

3.2 Dielectric analysis

Three specimens were prepared for any sample. All the specimens were stored in air-tight plastic bags at room temperature and measured after 28 day from production. Subsequently, one specimen for any sample was dried in an oven at 60 °C for 24 h and then measured again. This made it possible to measure them all on the same day. Another specimen was used for the time dependency test. Since the usage of the analyser would have lasted 24 h for each single sample, only 5 samples out of 9 were measured to reduce the time gap between the first and the last measurement. In particular, it was decided to measure the pristine cementitious matrix and the composites with the lowest and highest concentration: cement, cement/MWCNT(0.01 wt%), cement/MWCNT(0.50 wt%), cement/SWCNT(0.01 wt%), cement/SWCNT(0.50 wt%). More precise technical details about the EIS measurements were provided in Sect. 2.2.

3.2.1 Monitoring of the drying process

The real part of the conductivity (σ') was used to track the moisture reduction directly in the impedance spectrometer (Fig. 4). In fact, Wang and colleagues observed an exponential relationship between
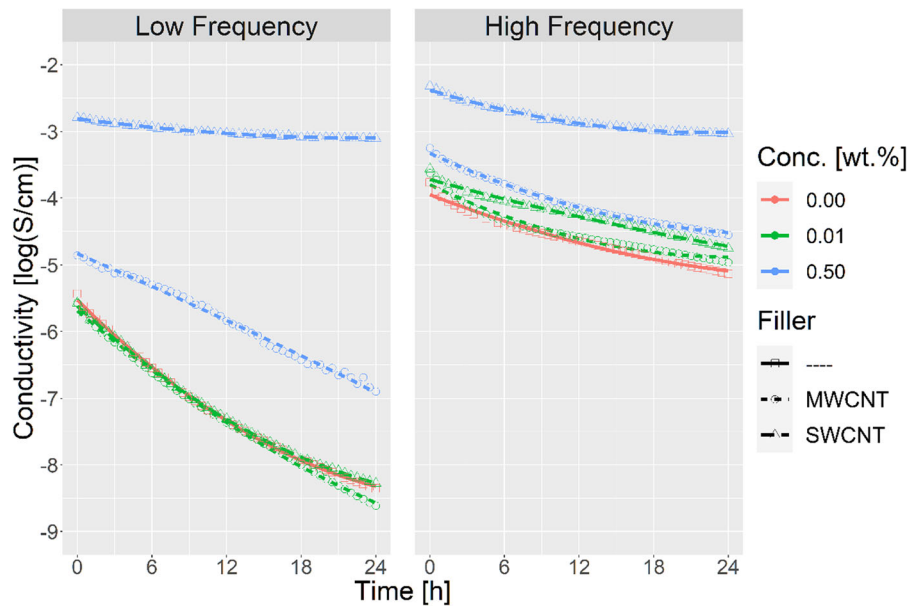
Fig. 4 Time dependency of the conductivity of the pristine cement and its CNT composites with various contents during 24 h of drying at 60 °C in air. Two frequencies are shown: 1.357 Hz (low frequency) and 1.317×10^6 Hz (high frequency). The dots show the experimental data, the colour lines define the concentration of filler while the shape of the dot or line shows its type

electrical resistance and water contents in carbon nanofiber cement mortar. [16] As expected, exposed at 60 °C and in a nitrogen flow, σ' consistently decreased over time. Close to the end of the measurement no plateaus were observed, meaning that the process did not stabilize after 24 h. The trend was clearly neither linear nor logarithmic, but a satisfying fitting of the data was found using a decay to base 10 function with the exponential parameter k expressed as a linear function of the time:

$$\sigma'(t) = \sigma_{t=0} 10^{-kt} \qquad (3)$$

$$k = at + b \qquad (4)$$

where σ' is the real part of the conductivity, $\sigma_{t=0}$ is the initial conductivity, t is the time, and k is the decay parameter expressed as a linear function of t, characterized by the parameters a and b. The values extrapolated from the fitting are given in Table 1. The higher the module of a, the higher is the deviation from the ideal decay process. The sign of a determines if k increases ($a > 0$) or decreases ($a < 0$) in time. The values of b provide a quantitative estimation of the speed of the initial phase of the conductivity-loss process, which tend to be more marked at low

frequency and for lower filler content. The trend of a as a function of the composition was less clear, but it seems to follow the same pattern of b. In time resolution, the faster initial loss was compensated by a faster tendency to the stabilization.

Observing the overall data, it was possible to conclude that a higher filler concentration resulted in a lower sensibility of the conductivity to moisture variations, in particular at low frequency. This already suggested that the moisture reduction on the one hand suppressed the ionic conductivity reducing the mobility of the electrolytes [7] while on the other hand the stripping out of water reduced the distances between the CNT and removed the veil of water wrapped around the fillers and filler agglomerates that prevented direct contact between the conductive particles as observed by the microscopes [8]. Such progressive concentration of the electrolytes in moisture was evidently the reason for the deviation from the ideal decay case. The level of dispersion of the filler clearly influenced $\log(\sigma_{t=0})$. SWCNTs formed clusters with higher aspect ratio than MWCNT, which provided a higher conductivity despite the worse dispersion, a characteristic observed also with other carbon fillers [36, 37]. The difference in dispersion of the fillers and

Table 1 Parameters extrapolated from the decay functions used for the fitting of the time dependency plot of σ

Frequency (Hz)	Filler (wt%)		a	b	$\log(\sigma_{t=0})$
1.357×10^{0}	–	–	− 0.891	5.76	− 7.19
	MWCNT	0.01	− 0.511	5.94	− 7.28
	MWCNT	0.50	− 0.082	4.29	− 5.84
	SWCNT	0.01	− 0.800	5.47	− 7.18
	SWCNT	0.50	− 0.161	0.60	− 3.00
1.317×10^{6}	–	–	− 0.320	2.35	− 4.61
	MWCNT	0.01	− 0.573	2.23	− 4.51
	MWCNT	0.50	− 0.476	2.45	− 4.06
	SWCNT	0.01	− 0.128	2.06	− 4.25
	SWCNT	0.50	− 0.397	1.30	− 2.81

the morphology of their agglomerates did not show a significant effect on the trend of the conductivity loss as a function of time. The morphology of the samples created an indirect effect because of the formation of a percolative network, which was only observable in the sample with 0.50 wt% SWCNT. The presence of a percolative network was connected to the higher aspect ratio of the clusters and caused a reduction in the influence of the water loss on the overall conductivity.

A higher dispersion of the CNTs in a matrix would have reduced the percolation concentration for both composites but not necessarily increased the σ'. As a matter of fact, once the percolation network is formed, a further increase of the filler dispersion does not significantly improve the conductivity [38]. The highest conductivity is usually achieved at a specific optimized dispersion degree, because when the primary particles are fully dispersed, they are completely surrounded by the matrix and the percolative paths are interrupted [36]. The use of defoamers and especially conductive dispersants partially prevents this trade off [39].

3.2.2 Difference between wet and dry states

By observing the conductivity of the samples as a function of the frequency (Fig. 5) it was possible to obtain more information on the role of nanofillers and moisture content with regard to the single phenomenon occurring in the conduction process. The introduction of the nanofillers did not just raise the curves (increase the conductivity) but also changed their shape. Moreover, the loss of humidity caused an evident change in the proportions. For the MWCNT

composites it was not possible to observe a percolation threshold. The values suggested the absence of any percolative network, since the conductivity remained low at lower frequency ranges. On the contrary, SWCNT composites showed a possible percolation threshold between 0.10 and 0.25 wt%. This transition was particularly evident in the dried composites since differences in conductivity were observed over several magnitudes. In fact, within the investigated range of frequency, only the two sample with the highest SWCNT loadings were presenting a region in which the conductivity was almost independent of the frequency, approaching the value of the DC. All other samples presented a transition region between AC and DC, with strong dependency of conductivity on the frequency. The higher percolation concentration of the MWCNT composites compared to the SWCNT might also be caused by the rounder shape of the agglomerates. Moreover, SWCNT agglomerates also showed a certain degree of alignment (Fig. 3) which was demonstrated in literature to influence the percolation concentration [40].

The complexity of these curves suggested that it was not possible to fit them with a single sigmoid like an ideal solid-state material. The fitting operation of these plots (Eq. 1) revealed the presence of three phenomena generating three different sigmoid, these were named α, β, and γ according to the position of their P_f (Eq. 1) on the frequency axis, proceeding from the lowest to the highest value. To verify this, the P_f of the found sigmoid was plotted as a function of the filler concentration for both SWCNT and MWCNT, in both dry and wet states (Fig. 6). Not all the sigmoid were present in all samples but they were clearly apparent in three sets. The P_f position was not
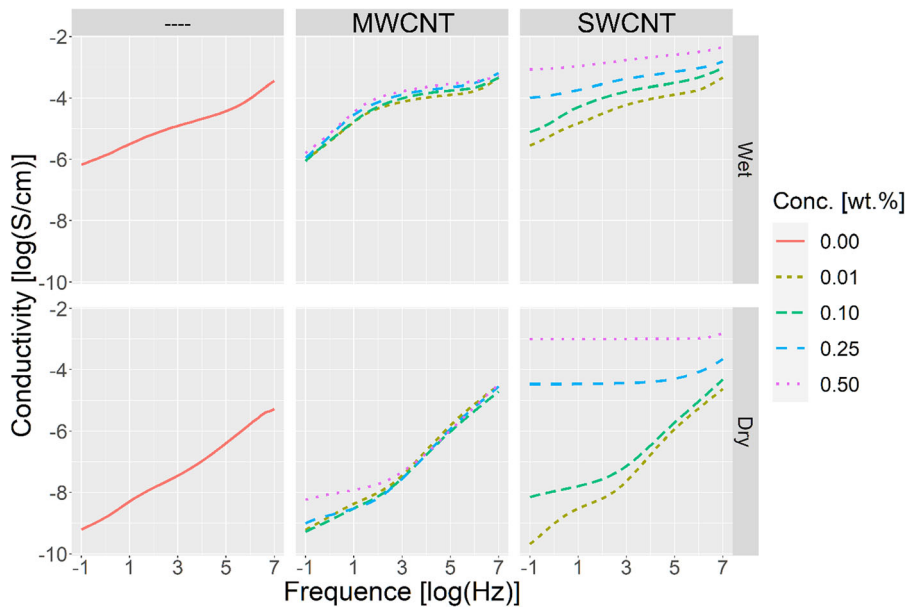
Fig. 5 Frequency dependent conductivity obtained from impedance spectroscopy before (top) and after (bottom) drying. On the left (top and bottom) is shown the pristine cement, in the centre and right its composites
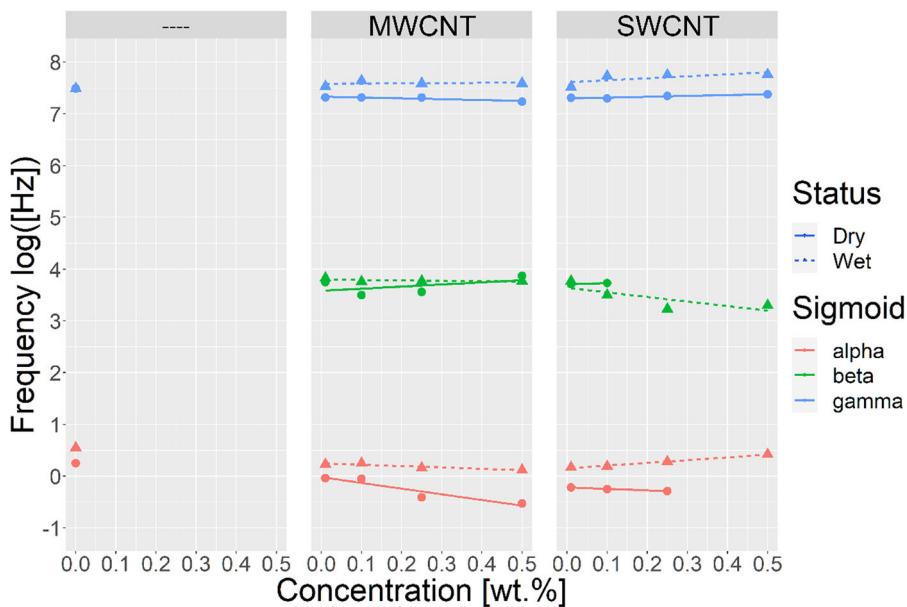

Fig. 6 Dependency of the flexural point frequency of the three sigmoid used in the fitting model on the concentration of CNT. On the left plot is shown the pristine cement, in centre and right its composites where the trends are highlighted with a linear interpolation line

constant, but a linear proportionality over concentration was observed.

The β-sigmoid was absent in the pristine cement suggesting a correlation to a polarization at the interface between the cement matrix and insulated

CNT. This phenomenon was observed in carbon nanofiber composites at similar frequencies [35] and has also been attributed to a dual layer polarization effect too weak to be detected in the pristine cement [27]. Interpolations of the pristine cement curves with

three sigmoid were tested but their RRS never showed an improvement over that obtained with only two sigmoid, suggesting that apparent bumps in the intermediate frequency range could be attributed to the overlap of the other phenomena (see Supporting information for the interpolation plots). A confirmation of the direct involvement of the carbon fillers was provided by the composites with 0.25 and 0.50 wt% of SWCNT. They showed a formed percolative network (Fig. 4), but the β-sigmoid was still present in the wet status, indicating a small but significant presence of insulated particles. The β-sigmoid only disappeared after drying, when the stripping of water from the inner volume of the specimen caused a shrinking of the sample with consequent reduction of the distances between the filler particles and then a reduction of the insulated SWCNT [41].

The α-sigmoid was attributed to the polarization phenomena occurring at the electrodes [42]. They were absent only in the dry sample with the highest concentration of SWCNT, where the direct contact between the electrode and the percolation network was more probable. In the wet corresponding sample, in fact, a layer of moisture could separate the exposed filler from the electrode [8]. The presence of moisture consistently moved the electrode polarization at higher frequencies, which can be explained by the introduction of an interphase layer between the electrode and the specimen.

The γ-sigmoid was attributed to the polarization phenomena between the cement particles, it was present in each sample without exception. [43] As with the α-sigmoid, the γ-sigmoid was shifted at higher frequency in the wet samples, confirming the presence of water in the volume of the samples, which was partially stripped out during the drying process. The position of γ-sigmoid was mostly independent of the filler content, which could indicate that interphases between CNTs and cement particle were relatively low in the bulk composite, as also seen in the microscopic analysis above. Moreover, this observation proved to be particularly true for the MWCNT where the surface contact between the filler and the matrix was significantly lower than in the SWCNT composite.

The contribution of the three sigmoid to the conductivity is represented in Fig. 7. Each bar is the mono-dimensional projection of the σ/f plots. The coloured sections into which each bar is divided represent the intensity of the change in conductivity caused by the specific polarization phenomenon. Mathematically, the length is the height of the sigmoid (Eq. 1). The reciprocal position of the sections was consistent: α at the bottom, β in the middle, and γ on the top. The bottom edge of the bars corresponds to the DC of the sample, while the AC is indicated by the top edge, as deduced by Eq. (2). All these values were also reported in Table 2.

In the pristine sample the AC conductivity was not influenced by the drying process and the polarization at the electrodes remained of almost the same intensity. However, the polarization at the bulk cement interfaces became more intense. One of the causes could be the reduced ion mobility as a consequence of the reduction of the aqueous conductive medium in the cementitious matrix. Another cause was the formation of micro voids, in addition to the voids already visible by the microscope, where water has evaporated.

Overall, the main characteristic that distinguished the composites with CNTs from the pristine cement was the β-sigmoid, which was related to the polarization effect at the interface matrix-filler. Only the fully insulated CNTs and CNT-agglomerates are involved in this phenomenon while those involved in a percolative net would quickly be discharged. For this reason, the β-sigmoid was not growing systematically in proportion to the CNT concentration. In fact, its intensity was influenced by the filler dispersion and which percentage of it was involved in the percolation. Theoretically, the higher form factor could affect the β-sigmoid in two opposite directions. On one side, a higher contact surface would have increased the polarization intensity, on the other side, it would have promoted the percolation network. Experimentally, it was observed that the second effect was dominant, since the SWCNT composites where the filler had a higher form factor, presented a β-sigmoid with lower intensity.

In the presence of CNTs, the γ-sigmoid decreased, which could also be attributed to two effects. One reason could be the influence of conductive fillers during the cement matrix preparation, causing the formation of fewer, bigger cementitious particles, with smaller interface extension. [44] Another reason could be the electron traps that conductive fillers exert on the surrounding matrix. [45] The drying process increased the γ-sigmoid height of the composites as already observed for the pristine cement.
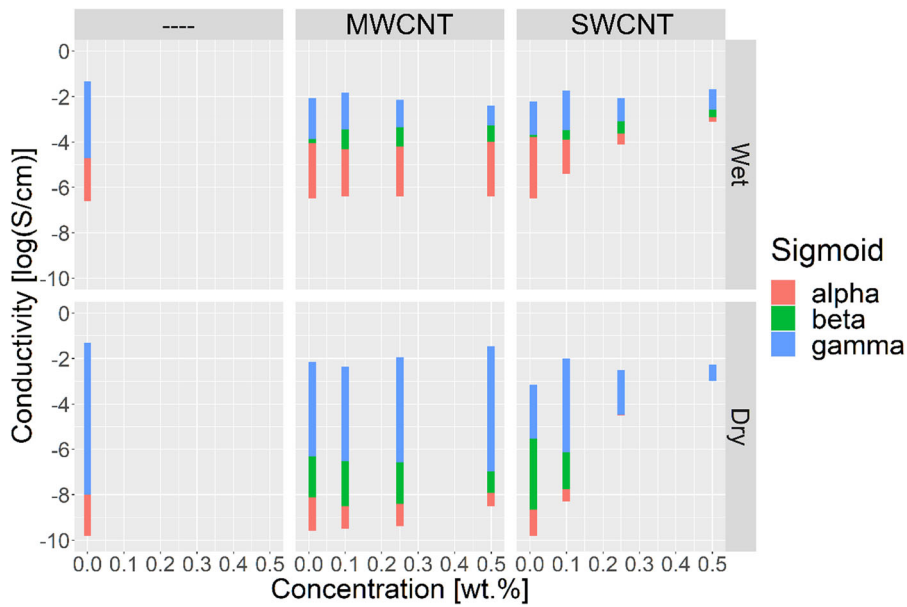
Fig. 7 One-dimensional projections of the Cole-plots of the pristine cement and its composites at various filler concentration, before and after drying, with the contributions of the sigmoid indicated by the colours

Table 2 Data extrapolated from the fitting of σ′ as a function of the *f* with a three sigmoid system

Status	Filler	Conc. (wt%)	Δ(log(σ_i))			DC (S/cm)	AC (S/cm)
			α (log (S/cm))	β (log (S/cm))	γ (log (S/cm))		
Dry	–	0.00	1.79	–	6.72	1.58×10^{-10}	5.11×10^{-2}
	MWCNT	0.01	1.48	1.81	4.15	2.51×10^{-10}	6.91×10^{-3}
		0.10	0.99	1.98	4.16	3.16×10^{-10}	4.26×10^{-3}
		0.25	0.99	1.84	4.62	3.98×10^{-10}	1.12×10^{-2}
		0.50	0.58	0.93	5.52	3.16×10^{-9}	1.24×10^{-2}
	SWCNT	0.01	1.13	3.15	2.37	1.58×10^{-10}	7.06×10^{-4}
		0.10	0.53	1.64	4.14	5.01×10^{-9}	1.02×10^{-2}
		0.25	0.03	–	1.95	3.16×10^{-5}	3.02×10^{-3}
		0.50	–	–	0.73	1.00×10^{-3}	5.37×10^{-3}
Wet	–	0.00	1.87	–	3.38	2.51×10^{-7}	4.46×10^{-2}
	MWCNT	0.01	2.44	0.19	1.8	3.16×10^{-7}	8.51×10^{-3}
		0.10	2.08	0.88	1.61	3.98×10^{-7}	1.48×10^{-2}
		0.25	2.2	0.86	1.2	3.98×10^{-7}	7.24×10^{-3}
		0.50	2.41	0.72	0.88	3.98×10^{-7}	4.07×10^{-3}
	SWCNT	0.01	2.71	0.11	1.46	3.16×10^{-7}	6.02×10^{-3}
		0.10	1.50	0.42	1.76	3.98×10^{-6}	1.90×10^{-2}
		0.25	0.47	0.55	1.03	7.94×10^{-5}	8.91×10^{-3}
		0.50	0.18	0.36	0.88	7.94×10^{-4}	2.09×10^{-2}

The order of magnitude of the contribution of each phenomenon and the current, direct and alternate (Eq. 1 and 2) for each sample is given

Compared to the pristine cement, the α-sigmoid height tended to decrease, moderately in the wet composites and more drastically after drying. This behaviour could be explained by the fact that the humidity veil prevented direct contact between the electrodes and the filler. Once removed, the charge accumulated could be more easily be discharged through the filler. In fact, the conductivity of the humidity layer was much lower than that of the gold of the electrode and of the CNTs in the composites, causing the formation of local capacitors between the electrode and the fillers, which were carrying a higher electron density then the matrix around [46]. After drying, this veil was removed, and the capacitors mostly disappeared.

The comparison between MWCNT and SWCNT composites evidenced the pivotal role of the formation of a percolative network. While the sample with 0.01 and 0.10 wt% filler content showed a similar behaviour independently of the CNTs, concentrations over the SWCNT percolation threshold created a complete differentiation between the two series of samples. The main effect of the percolation in the wet samples was a drastic reduction of the polarisation at the electrodes and at the matrix particles interface, because the charges that would have previously accumulated, could now be dissipated. On the contrary, almost no effect was observed on the matrix-filler interface, because of the contribution of residual insulated CNT particles. After drying, all the described effects intensified, so much so that the matrix-filler polarization completely fell under the detection limit. This behaviour suggests that the water stripped from inside the volume of the sample caused a shrinking of the composite and a consequent reduction of the distances between the filler particles. This also resulted in a progressive increase of the DC which reached a maximum of 10^{-3} S/cm in the sample with 0.50 wt%, where the only detectable sigmoid was caused by a residual polarization of the matrix particles.

These results showed that a variation of conductivity in a sensing device can have different causes: a variation of the moisture as a consequence of the atmospheric conditions, a crack in the structure that interrupts the CNT percolative network, a deterioration of the surface of the electrodes in the device or the measurement instrument, and more. These issues will have different effects on the conductive phenomena observed with the three sigmoid, some more predictable, other less. Being able to distinguish the specific cause of an emerging problem would simplify and shorten the process of resolving it.

4 Conclusions

Classical OPC and its composites with SWCNT and MWCNT were prepared and measured with impedance spectroscopy to define the phenomena of electrical conduction. The measurements were performed before, after, and during a drying process to examine the effect of the moisture and to quantitatively describe the kinetics of the process itself by observing the change in conductivity. This work provided the basis for applying these multifunctional materials for sensing mechanical loads, moisture, temperature etc. In fact, profiling the conductivity variation as a function of time and frequency, has shown them be characteristic of different causes. By disaggregating and quantifying change in conductivity, it would be possible to speed up the identification and resolution of root causes in eventual applications.

It was found that a simple decay model could not adequately describe the drying process since the initial decay process slowed down proportionally with the time. This behaviour was attributed to the fact that in the beginning the water was mostly removed from the external surface of the specimen, since the internal water needed more time to be stripped out. Subsequently, the process gradually slowed down. Within the investigated time, this change could be efficiently described by a stretched exponential factor. In 24 h this process did not reach any plateau.

In the pristine cement sample two polarization phenomena were observed, one at the electrode-specimen interface and the second at the interfaces between the cement phases, clearly visible via the microscope. In the composites, a third polarization effect appeared at the interface between the filler and the matrix and disappeared again in the samples with a fully formed percolated network: dried samples with 0.25 and 0.50 wt% SWCNT.

The insulating effects of humidity veils between the specimen and the electrodes were easily removed by drying. In particular, these veils were observable in the presence of CNTs, since the carbon filler and the gold electrode had a much higher conductivity than the humidity layer in between. The electrode polarization

was the phenomenon most affected by the drying process, because the water involved was at the surface of the specimen, where it was more easily removed. In the bulk specimen instead, the polarisation increased at the cement phase boundaries, probably due to the formation of microcavities. The moisture reduction caused a shift of these two phenomena to a higher frequency due to the reduction of the mobility of the electrolytes. No evident effect was observed on the matrix-filler interface.

The electrical percolation had the effect of decreasing all the polarization phenomena, since the conductive net could dissipate the accumulated charges. The removal of the moisture enhanced this effect to the point that only a small polarization effect at the cementitious particle–particle interfaces remained. In fact, the transition between non-percolative and percolative systems became more defined after the conductive effect of the moisture disappeared.

To conclude, the two kinds of binary materials investigated, percolative and non-percolative, seemed to be useful for different applications. The percolative material was more suitable to the detection of mechanical failures, since the electrical percolation overlaid the other conductive phenomena. The non-percolative material seemed more appropriate for corrosion and chemical alteration detection. This study was limited to classical OPC, but the obtained results might be generalised to other classes of matrices like geopolymers or other alkaline activated materials, while other kinds of fillers or ternary composites will require a separate study. Furthermore, studies of the calibration, detection limits, and ecological and financial impacts of the sensing device must be performed for specific applications.

Declarations

Conflict of interest   The authors declare that they have no known competing financial interest or personal relationships that could have appeared to influence the work reported in this paper.

References

1. Dong W, Li W, Tao Z, Wang K (2019) Piezoresistive properties of cement-based sensors: review and perspective. Constr Build Mater 203:146–163. https://doi.org/10.1016/j.conbuildmat.2019.01.081

2. Raki L, Beaudoin J, Alizadeh R, Makar J, Sato T (2010) Cement and concrete nanoscience and nanotechnology. Materials 3:918–942. https://doi.org/10.3390/ma3020918

3. Al-Rub RKA, Ashour AI, Tyson BM (2012) On the aspect ratio effect of multi-walled carbon nanotube reinforcements on the mechanical properties of cementitious nanocomposites. Constr Build Mater 35:647–655. https://doi.org/10.1016/j.conbuildmat.2012.04.086

4. Saafi M, Andrew K, Tang PL, McGhon D, Taylor S, Rahman M, Yang S, Zhouc X (2013) Multifunctional properties of carbon nanotube/fly ash geopolymeric nanocomposites. Constr Build Mater 49:46–55. https://doi.org/10.1016/j.conbuildmat.2013.08.007

5. Zhang L, Ding S, Lia L, Dong S, Wang D, Yu X, Han B (2018) Effect of characteristics of assembly unit of CNT/NCB composite fillers on properties of smart cement-based materials. Compos A Appl Sci Manuf 109:303–332. https://doi.org/10.1016/j.compositesa.2018.03.020

6. Han B, Zhang K, Yu X, Kwon E, Ou J (2012) Electrical characteristics and pressure-sensitive response measurements of carboxyl MWNT/cement composites. Cem Concr Compos 34:794–800. https://doi.org/10.1016/j.cemconcomp.2012.02.012

7. Liebscher M, Tzounis L, Junger D, Dinh TT, Mechtcherine V (2020) Electrical Joule heating of cementitious nanocomposites filled with multi-walled carbon nanotubes: role of filler concentration, water content, and cement age. Smart Mater Struct 29:125019. https://doi.org/10.1088/1361-665X/abc23b

8. Tzounis L, Liebscher M, Fuge R, Leonhardt A, Mechtcherine V (2019) p- and n-type thermoelectric cement composites with CVD grown p- and n-doped carbon nanotubes: demonstration of a structural thermoelectric

generator. Energy Build 191:151–163. https://doi.org/10.1016/j.enbuild.2019.03.027

9. Materazzi AL, Ubertini F, D'Alessandro A (2013) Carbon nanotube cement-based transducers for dynamic sensing of strain. Cem Concr Compos 37:2–11. https://doi.org/10.1016/j.cemconcomp.2012.12.013

10. Zmeskal O, Trhlikova L, Pospisil J, Fiala L, Florian P (2020) Investigation of electric and thermal properties of alkali-activated aluminosilicates with a cnt admixture. Ceram Silik 64:180–189. https://doi.org/10.13168/cs.2020.0007

11. Asami K (2002) Characterization of heterogeneous systems by dielectric spectroscopy. Prog Polym Sci 27:1617–1659. https://doi.org/10.1016/S0079-6700(02)00015-1

12. Chaipanich A, Rianyoi R, Potong R, Suriya W, Jaitanong N, Chindaprasirt P (2012) Dielectric properties of 2–2 PMN-PT/cement composites. Ferroelectr Lett Sect 39:76–80. https://doi.org/10.1080/07315171.2012.738595

13. Potong R, Rianyoi R, Jareansuk L, Jaitanong N, Yimnirun R, Chaipanich A (2010) Effect of particle size on dielectric and ferroelectric properties of 0–3 lead magnesium niobate titanate-portland cement composites. Ferroelectrics 405:98–104. https://doi.org/10.1080/00150193.2010.482899

14. Chaipanich A, Rianyoi R, Potong R, Jaitanong N (2010) Effect of temperature on the dielectric properties of 0–3 PZT-cement composites. Ferroelectr Lett Sect 37:76–81. https://doi.org/10.1080/07315171.2010.527799

15. Jaitanong N, Yimnirun R, Chaipanich A (2009) Effect of uniaxial stress on dielectric properties of 0–3 PZT-Portland cement composite. Ferroelectrics 384:174–181. https://doi.org/10.1080/00150190902881470

16. Wang H, Zhang A, Zhang L, Wang Q, Yang X-H, Gao X, Shi F (2020) Electrical and piezoresistive properties of carbon nanofiber cement mortar under different temperatures and water contents. Constr Build Mater 265:120740. https://doi.org/10.1016/j.conbuildmat.2020.120740

17. da Silva GF, Martini S, Moraes JCB, Teles LK (2021) AC impedance spectroscopy (AC-IS) analysis to characterize the effect of nanomaterials in cement-based mortars. Constr Build Mater 269:121260. https://doi.org/10.1016/j.conbuildmat.2020.121260

18. Díaz B, Guitián B, Nóvoa XR, Pérez C (2021) Conductivity assessment of multifunctional cement pastes by impedance spectroscopy. Corros Sci 185:109441. https://doi.org/10.1016/j.corsci.2021.109441

19. Li L, Zhang Y, Hubler MH, Xi Y (2021) Experimental study on nanoparticle injection technology for remediating leaks in the cement from wellbore systems. J Pet Sci Eng J Petrol Sci Eng 203:108829. https://doi.org/10.1016/j.petrol.2021.108829

20. Levita G, Marchetti A, Gallone G, Princigallo A, Guerrini GL (2000) Electrical properties of fluidified Portland cement mixes in the early stage of hydration. Cem Concr Res 30:923–930. https://doi.org/10.1016/S0008-8846(00)00282-9

21. Tian W, Liu Y, Wang W (2021) Multi-structural evolution of conductive reactive powder concrete manufactured by enhanced ohmic heating curing. Cem Concr Compos 123:104199. https://doi.org/10.1016/j.cemconcomp.2021.104199

22. García-Macías E, Rodríguez-Tembleque L, Sáez A (2018) Bending and free vibration analysis of functionally graded graphene vs. carbon nanotube reinforced composite plates. Compos Struct 186:123–138. https://doi.org/10.1016/j.compstruct.2017.11.076

23. Yang P, Chowdhury S, Neithalath N (2018) Strain sensing ability of metallic particulate reinforced cementitious composites: experiments and microstructure-guided finite element modeling. Cem Concr Compos 90:225–234. https://doi.org/10.1016/j.cemconcomp.2018.04.004

24. Potong R, Rianyoi R, Chaipanich A (2010) Dielectric properties of lead-free composites from 0–3 barium zirconate titanate-portland cement composites. Ferroelectr Lett Sect 133:18–23. https://doi.org/10.1080/07315171.2011.570176

25. Funke K, Banhatti RD (2005) Conductivity spectroscopy covering 17 decades on the frequency scale. Solid State Ion 176:1971–1978. https://doi.org/10.1016/j.ssi.2004.06.029

26. Zhang J, Heath A, Abdalgadir HMT, Ball RJ, Paine K (2022) Electrical impedance behaviour of carbon fibre reinforced cement-based sensors at different moisture contents. Constr Build Mater 353:129049. https://doi.org/10.1016/j.conbuildmat.2022.129049

27. Hawreen A, Bogas JA (2019) Creep, shrinkage and mechanical properties of concrete reinforced with different types of carbon nanotubes. Constr Build Mater 198:70–81. https://doi.org/10.1016/j.conbuildmat.2018.11.253

28. Fuge R, Liebscher M, Schröfl C, Leonhardt A, Mechtcherine V (2016) Fragmentation characteristics of undoped and nitrogen-doped multiwalled carbon nanotubes in aqueous dispersion in dependence on the ultrasonication parameters. Diam Relat Mater 66:126–134. https://doi.org/10.1016/j.diamond.2016.03.026

29. Liebscher M, Gärtner T, Tzounis L, Mičušík M, Pötschke P, Stamm M, Heinrich G, Voit B (2014) Influence of the MWCNT surface functionalization on the thermoelectric properties of melt-mixed polycarbonate composites. Compos Sci Technol 101:133–138. https://doi.org/10.1016/j.compscitech.2014.07.009

30. Liebscher M, Tzounis L, Pötschke P, Heinrich G (2013) Influence of the viscosity ratio in PC/SAN blends filled with MWCNTs on the morphological, electrical, and melt rheological properties. Polymer 54:6801–6808. https://doi.org/10.1016/j.polymer.2013.10.040

31. Jazaei R, Karakouzian M, O'Toole B, Moond J, Gharehdaghid S (2022) Energy dissipation capacity of cementitious nanocomposite reinforced by hybrid carbon nanotubes. Constr Build Mater 323:126396. https://doi.org/10.1016/j.conbuildmat.2022.126396

32. Kasaliwal GR, Pegel S, Göldel A, Pötschke P, Heinrich G (2010) Analysis of agglomerate dispersion mechanisms of multiwalled carbon nanotubes during melt mixing in polycarbonate. Polymer 51:2708–2720. https://doi.org/10.1016/j.polymer.2010.02.048

33. Díaz B, Guitián B, Nóvoa XR, Pérez C (2020) Analysis of the microstructure of carbon fibre reinforced cement pastes by impedance spectroscopy. Constr Build Mater 243:118207. https://doi.org/10.1016/j.conbuildmat.2020.118207

34. Liebscher M, Dinh TT, Schröfl C, Mechtcherine V (2020) Dispersion of different carbon-based nanofillers in aqueous

suspension by polycarboxylate comb-type copolymers and their influence on the early age properties of cementitious matrices. Constr Build Mater 241:118039. https://doi.org/10.1016/j.conbuildmat.2020.118039

35. Gwon S, Moon J, Shin M (2022) Self-heating capacity of electrically conductive cement composites: effects of curing conditions. Constr Build Mater 353:129087. https://doi.org/10.1016/j.conbuildmat.2022.129087

36. Piana F, Pionteck J (2013) Effect of the melt processing conditions on the conductive paths formation in thermoplastic polyurethane/expanded graphite (TPU/EG) composites. Compos Sci Technol 80:39–46. https://doi.org/10.1016/j.compscitech.2013.03.002

37. Liebscher M, Domurath J, Saphiannikova M, Mueller MT, Heinrich G, Pötschke P (2020) Dispersion of graphite nanoplates in melt mixed PC/SAN polymer blends and its influence on rheological and electrical properties. Polymer 200:122577. https://doi.org/10.1016/j.polymer.2020.122577

38. Hongyu S, Binmeng C, Bo L, Shengwen T, Zongji L (2017) Influence of dispersants on the properties of CNTs reinforced cement-based materials. Constr Build Mater 131:186–194. https://doi.org/10.1016/j.conbuildmat.2016.11.053

39. Choi K, Min YK, Chung W, Lee S-E, Kang S-W (2020) Effects of dispersants and defoamers on the enhanced electrical performance by carbon nanotube networks embedded in cement-matrix composites. Compos Struct 243:112193. https://doi.org/10.1016/j.compstruct.2020.112193

40. Cob J, Oliva-Avilés AI, Avilés F, Oliva AI (2019) Influence of concentration, length and orientation of multiwall carbon nanotubes on the electromechanical response of polymer nanocomposites. Mater Res Express 6:115024. https://doi.org/10.1088/2053-1591/ab447b

41. Mastali M, Kinnunen P, Dalvand A, Firouz RM, Illikainen M (2018) Drying shrinkage in alkali-activated binders—a critical review. Constr Build Mater 190:533–550. https://doi.org/10.1016/j.conbuildmat.2018.09.125

42. Torrents JM, Mason TO, Garboczi EJ (2000) Impedance spectra of fiber-reinforced cement-based composites: a modeling approach. Cem Concr Res 30:585–592. https://doi.org/10.1016/S0008-8846(00)00211-8

43. Phromviyo N, Sirikamalat S, Chanlek N, Thongbai P, Amornkitbamrung V, Chindaprasirt P (2020) Significantly improved non-ohmic and giant dielectric response in $CaCu_3Ti_4O_{12}$ ceramics by incorporating Portland cement. Mater Res Express 7:066301. https://doi.org/10.1088/2053-1591/ab98cb

44. Huang H, Teng L, Gao X, Khayat KH, Wang F, Liuac Z (2022) Effect of carbon nanotube and graphite nanoplatelet on composition, structure, and nano-mechanical properties of C-S-H in UHPC. Cem Concr Res 154:106713. https://doi.org/10.1016/j.cemconres.2022.106713

45. Chandra KS, Pandurangan A (2014) Fabrication of solution processed carbon nanotube embedded polyvinyl alcohol composite film for non-volatile memory device. J Nanosci Nanotechnol 14:2381–2387. https://doi.org/10.1166/jnn.2014.8489

46. Alread JM, Bets KV, Xie Y, Yakobson BI (2018) Machine learning electron density in sulfur crosslinked carbon nanotubes. Compos Sci Technol 166:3–9. https://doi.org/10.1016/j.compscitech.2018.03.035